TRENDS IN SCIENCES 2026; 23(12): 14111
https://doi.org/10.48048/tis.2026.14111 RESEARCH ARTICLE

Effect of Hydroxyl–Carboxyl Positional Isomerism in Hydroxybenzoic Acids on Gold Nanoparticle Capping and Paraquat Binding

Wianthi Septia Witasari[1,2], Adhitasari Suratman[1] and Sri Juari Santosa[1,*]

[1]*Department of Chemistry, Universitas Gadjah Mada, Yogyakarta 55281, Indonesia*
[2]*Department of Chemical Engineering, Politeknik Negeri Malang, Jawa Timur 65141, Indonesia*

([*]Corresponding author's e-mail: sjuari@ugm.ac.id)

Received: 18 April 2026, Revised: 29 May 2026, Accepted: 8 June 2026, Published: 30 July 2026

Abstract

The positions of hydroxyl and carboxyl groups in hydroxybenzoic acid (HBA) isomers strongly influence their molecular properties; however, their roles in nanoparticle capping and analyte interactions remain insufficiently understood. This study aims to investigate how the positional isomerism of *o*–, *m*–, and *p*–hydroxybenzoic acid affects the synthesis, colloidal stability, and paraquat binding properties of gold nanoparticles (AuNPs). AuNPs were synthesized using each hydroxybenzoic acid isomer as a dual reducing and capping agent. UV–Vis spectroscopy, TEM, DLS, zeta potential, FTIR, and XRD characterized the resulting nanoparticles. Paraquat interactions were evaluated through SPR, hydrodynamic size, and aggregation changes at 1×10^{-4} M to 1×10^{-3} M. *o*–hydroxybenzoic acid produces the smallest (22.28 nm) and most uniform AuNPs with the highest negative zeta potential (-52.8 mV), which may be related to intramolecular hydrogen bonding. Upon paraquat exposure, *o*-hydroxybenzoic acid-capped AuNPs showed the most pronounced SPR red shift and the largest increase in hydrodynamic diameter (46.76 to 92.55 nm). *m*–hydroxybenzoic acid-capped AuNPs exhibited intermediate responses, while *p*–hydroxybenzoic acid–capped AuNPs showed the weakest plasmonic response. Positional isomerism of hydroxybenzoic acids governs AuNPs formation, and paraquat induces aggregation. Despite their higher intrinsic stability, *o*–hydroxybenzoic acid-capped AuNPs are the most responsive to paraquat, which is proposed to involve π–π donor–acceptor interactions. These findings provide insight into the role of positional isomerism for designing isomer-selective capping layers in nanoparticle-based detection systems.

Keywords: Gold nanoparticles, Hydroxybenzoic acid isomers, Paraquat, π–π interaction, Positional isomerism

Introduction

Gold nanoparticles (AuNPs) have received significant attention in materials science, chemistry, and biotechnology due to their unique Localized Surface Plasmon Resonance (LSPR) properties [1]. This optical phenomenon, highly sensitive to particle size, shape, and aggregation state, enables powerful applications in spectroscopy, sensing, and colorimetric detection [2–6]. LSPR arises from the collective oscillation of conduction electrons at the nanoparticle surface when excited by light, leading to a strong absorption band in the visible to near infrared region. In sensing, LSPR shift induced by analyte binding or nanoparticle aggregation enables rapid, label-free, and often colorimetric detection that can be observed visually or quantified with simple spectrophotometry [7]. The practicality of AuNPs-based colorimetric biosensors, characterized by their low cost, minimal instrumentation requirements, and adaptability to a wide range of analytes, makes LSPR transduction a leading approach for efficient and accessible chemical and biological sensing [1,7].

Small phenolic compounds can serve a dual function, reducing Au^{3+} to Au^{0} and simultaneously capping the resulting AuNPs. This bifunctional role aligns with green chemistry principles by minimizing reagent use and simplifies surface functionalization for targeted applications [9]. Hydroxybenzoic acids, especially the *ortho*– (*o*–hydroxybenzoic), *meta*–

(*m*–hydroxybenzoic), and *para*– (*p*–hydroxybenzoic), are a class of bifunctional organic molecules featuring both a phenolic (–OH) and carboxylic acid (–COOH) group attached to a benzene ring. Their phenolic –OH groups can donate electrons (reduction), while carboxylic groups coordinate to the Au surface, providing colloidal stabilization [10]. State-of-the-art routes to colloidal AuNPs include citrate or ascorbate reductions (Turkevich type), seed-mediated growth, photochemical/electrochemical methods, and biogenic/organic small molecule reduction that eliminate surfactants and harsh reagents [2,8,11]. Compared with amino acid or polymer reductants, hydroxybenzoic acid isomers offer simple, single-step synthesis in aqueous media. These isomers provide intrinsic surface functional groups ($–COO^-$/$–O^-$) that ensure colloidal stability without additional ligands. Furthermore, this approach provides cleaner surface chemistry, which enhances both reproducibility and downstream analyte interaction [9–11].

The chemical behaviour of hydroxybenzoic acid isomers is influenced by the relative position of these substituents, which dictates molecular properties such as electron density distribution, planarity, intramolecular interactions, and conformational flexibility. These differences make them versatile yet distinct reducing and capping agents in the synthesis of metal nanoparticles, particularly AuNPs. The unique characteristic of *o*–hydroxybenzoic acid is its ability to form a strong, resonance-stabilized intramolecular hydrogen bond between the neighboring –OH and –COOH groups [12]. This interaction, confirmed by gas-phase electron diffraction studies, locks the carboxyl group coplanar with the benzene ring and results in a rigid, cyclic structure [12]. This bonding shortens the phenolic C–O bond and influences the electron density across the molecule [12,13]. In contrast, *m*– and *p*–hydroxybenzoic cannot form such an internal hydrogen bond due to the greater separation between functional groups. *m*–hydroxybenzoic exhibits no special intramolecular interaction, while *p*–hydroxybenzoic possesses a symmetric structure that allows for resonance delocalization across the entire molecule, enhancing stability [14]. On the other hand, *o*–hydroxybenzoic acid is stable as a single conformer at laboratory temperature because of an internal hydrogen bond. In contrast, *m*– and *p*–hydroxybenzoates exist as mixtures of multiple conformers due to the rotation of the carboxyl and hydroxyl groups [12]. These fundamental differences have practical implications in nanoparticle synthesis and subsequent molecular interactions.

Paraquat is a widely used, cationic bipyridyl herbicide that carries a divalent positive charge ($^{2+}$). It is highly toxic and can induce electrostatic aggregation of negatively charged, carboxylate-capped AuNPs, resulting in a distinct color change observable by the naked eye [15]. Despite its agronomic efficiency and low cost, paraquat poses notable environmental concerns due to its persistence and strong adsorption onto soil and sediment particles, which hinder biodegradation and promote long-term accumulation [16]. Its environmental toxicity has been reported extends beyond target species, affecting algae, aquatic invertebrates, and birds even at sublethal concentration, and potential bioaccumulation through food webs has been reported [16,17]. Moreover, chronic exposure in humans has been associated with pulmonary fibrosis, renal dysfunction, and a possible link to neurodegenerative diseases such as Parkinson [18,19].

Although hydroxybenzoic acids have previously been employed as reducing and capping agents for AuNPs synthesis, the influence of hydroxybenzoic–carboxyl positional isomerism on nanoparticle paraquat-induced aggregation has not been systematically investigated. In particular, the relationship between hydroxybenzoic acid–capped AuNPs and cationic analytes such as paraquat remains insufficiently understood. Furthermore, the relative contribution of π–π donor-acceptor interaction and electrostatic interactions in mediating paraquat-induced aggregation has not been clearly elucidated. Therefore, this study aims to correlate the positional isomerism of *o*–, *m*– and *p*–hydroxybenzoic acids with AuNPs formation, and paraquat induced optical responses to provide fundamental insight into the interaction behaviour of hydroxybenzoic acids capped AuNPs system. The mechanistic insights gained from this fundamental interaction study are expected to provide a foundational basis for the future development of colorimetric sensors for paraquat detection, particularly through the rational selection of capping agent isomers.

Materials and methods

Materials

Chloroauric Acid ($HAuCl_4$) was purchased from Smart Lab, *o*–hydroxybenzoic acid, *p*–hydroxybenzoic acid, sodium hydroxide from Merck, *m*–hydroxybenzoic acid from Sigma Aldrich, and paraquat dichloride hydrate from Supelco. All chemicals were used as received without any further purification. Double-distilled water was used in all experiments. SPR spectra were measured using UV–Visible spectrophotometer (Shimadzu UV–1700). Fourier transmission infrared spectrophotometer (Simadzu FTIR Prestige–21) was used to investigate the interaction of AuNPs surface with hydroxybenzoic acid isomers. A transmission electron microscope (TEM, JEOL JEM–1400) was used to determine the size and morphology of AuNPs. The hydrodynamic diameter and zeta potential of the AuNPs were characterized using Horiba SZ-100 instrument. X-ray diffraction (XRD) patterns were acquired on a Shimadzu XRD-6000 diffractometer with Cu K_α radiation (λ = 1.5418 Å) at 40 kV and 30 mA to investigate the crystal structure. Diffractograms were recorded across a 2θ range of 10° - 80° at a scan rate of 4° per min.

Methods

AuNPs synthesis was performed according to Turkevich's simplified method [20] by mixing $HAuCl_4$ 2.1×10^{-7} M and capping agents (*o*–, *m*–, and *p*–hydroxybenzoic acids) 1.0×10^{-2} M in a 1:1 volume ratio in a water bath at 98 °C, and the incubation time was 20 min. The pH of hydroxybenzoic acid is optimized (1.0 - 12.0) to evaluate the effect of pH on the synthesis product.

SPR absorption spectra were recorded using a UV-Vis spectrophotometer. All UV–Vis measurements were carried out at room temperature within a wavelength range of 350 - 800 nm using a quartz cuvette with a 1 cm path length. Solid samples for Fourier Transmission Infrared Spectrophotometer (FTIR) and X-Ray Diffraction (XRD) analysis were obtained from colloidal suspensions by centrifugation at 8,000 rpm and drying in an oven at 70 °C. FTIR spectra were recorded using the KBr pellet technique over a scanning range of 400 - 4,000 cm^{-1}. Samples for Transmission Electron Microscope (TEM) analysis were prepared by immersing a copper grid into the colloidal AuNPs dispersion and drying at room temperature. TEM images were acquired at an accelerating voltage of 120 kV, and particle size distributions were determined using the scale indicated on the micrographs. Particle size distribution and hydrodynamic diameter of the synthesized AuNPs were further analyzed using Particle Size Analyzer (PSA) based on Dynamic Light Scattering (DLS) measurements at room temperature. Zeta potential measurements were also performed to evaluate the surface charge and colloidal stability of AuNPs suspensions.

For paraquat interaction studies, 1 mL of paraquat solution with concentrations ranging from 1×10^{-4} M - 1×10^{-3} M was added to the 2 mL hydroxybenzoic acids capped AuNP colloidal solution under ambient conditions. The mixtures were gently homogenized for 50 min prior to UV-Vis, TEM and DLS measurements to evaluate plasmonic response and aggregation behaviour.

Result and discussion

Synthesis and characterization of AuNPs

UV-Vis spectrophotometer

The synthesis of AuNPs using hydroxybenzoic acid (HBA) isomers as dual function agents (reducing and capping) highlights the crucial role of functional groups in nanoparticle nucleation and growth. UV–Vis spectra of three capped gold nanoparticle systems, synthesized using the three hydroxybenzoic acid isomers as reducing and stabilizing agents, exhibited characteristic SPR band in the region of 526 - 536 nm, which corresponds to the LSPR typical for spherical AuNPs. The spectral data in **Figure 1** reveal distinct pH dependent trends in SPR absorbance among the isomers. Specifically for *o*–hydroxybenzoic acid, maximum stability and sharpest LSPR absorbance were observed at pH 11, as indicated by the highest absorbance values (1 a.u.) at wavelengths from 400 - 650 nm, along with minimal spectral broadening. In contrast, *m*–hydroxybenzoic acid and *p*–hydroxybenzoic acid demonstrated optimal nanoparticle reduction and stabilization at pH 10, where absorbance peaks were most defined and showed reduced broadening compared to other pH conditions. These variations in optimal pH reflect the positional influence of the hydroxyl and carboxyl groups on each isomer's electron-donating

capacity and adsorption behavior on the nanoparticle surface, which in turn affects nanoparticle size distribution, dispersity, and aggregation state. Narrower, blue-shifted SPR bands correlate with smaller and more monodisperse particles, whereas broader, red-shifted profiles suggest larger or aggregated populations [21].

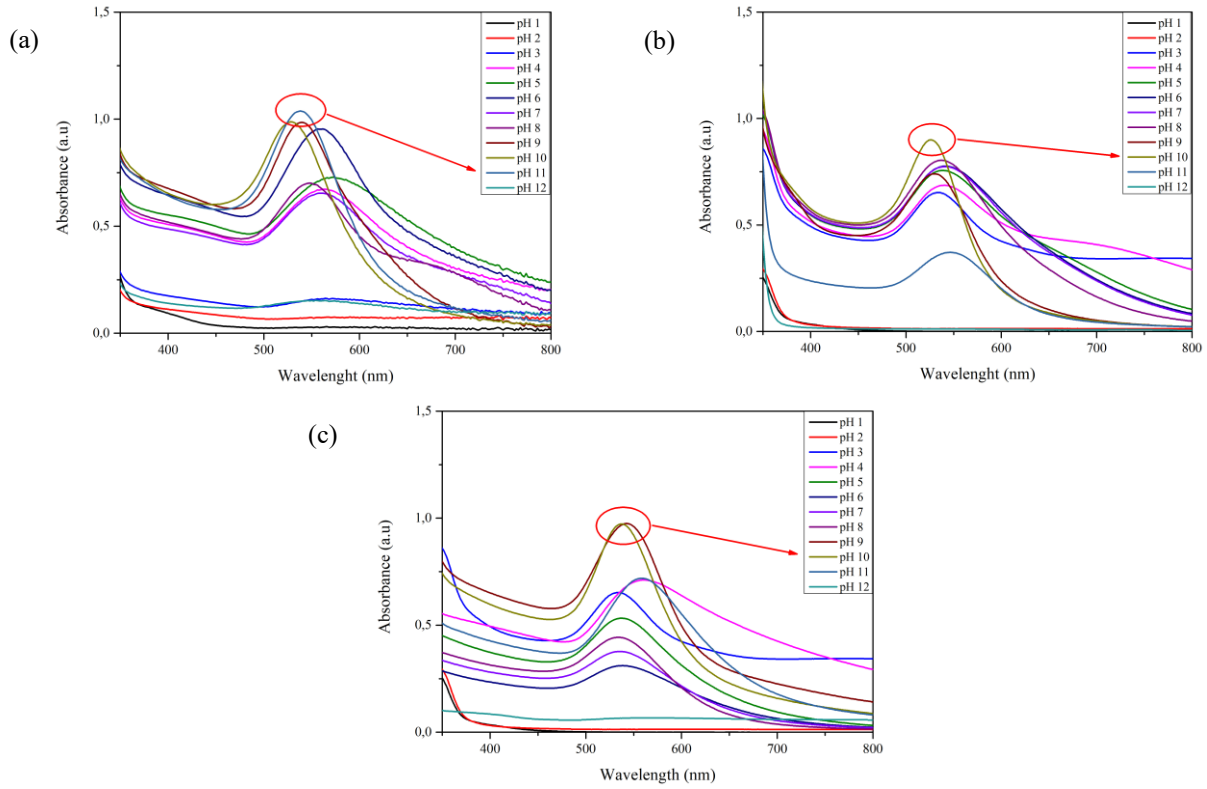


Figure 1 SPR spectra of AuNPs at different pH of hydroxybenzoic acid isomers, 2.1×10^{-7} M Au^{3+}, 1.0×10^{-2} M hydroxybenzoic acid isomers, 20 min reaction time, (a) *o*–hydroxybenzoic acid, (b) *m*–hydroxybenzoic, (c) *p*–hydroxybenzoic acid.

The hydroxyl (–OH) groups in hydroxybenzoic provide lone pairs of electrons, which can be donated to Au^{3+} ions, thus facilitating their reduction to elemental gold (Au^0). The carboxylate ($–COO^-$) groups act as surface capping agents via electrostatic or coordinative interaction, preventing uncontrolled particle growth and aggregation. These two functions make hydroxybenzoic acid highly attractive for environmentally friendly and practical AuNPs synthesis compared to traditional chemical reducing agents, which often require toxic reagents and harsh conditions [10,22,23]. The relative position (*o*–, *m*–, and *p*–) of the hydroxyl and carboxyl substituent influences the electron density, chelation ability, and hydrogen bonding patterns, which ultimately determine the reduction kinetics, particle size distribution, and colloidal stability. These molecular-level structural differences provide the basis for understanding the variations in optical properties and sensing performance of hydroxybenzoic acid-derived AuNPs. This finding is consistent with previous reports showing that polyphenolic and aromatic carboxylates exhibit efficient metal ion reduction while stabilizing nanoparticles through surface binding, respectively, sensing and catalytic applications [10,24].

The ortho isomer, which contains neighboring –OH and –COOH groups, exhibits unique intramolecular interactions (**Figure 2**) compared to its meta and para counterparts. The close proximity of these functional groups allows the formation of intramolecular hydrogen bonding, which stabilizes the molecular structure and consequently affects its acid-base behavior. For all isomers, pKa_1 corresponds to the dissociation constant of the carboxyl group (–COOH), while pKa_2 represents the dissociation constant of the phenolic hydroxyl group (–OH). In *o*–hydroxybenzoate acid, the proximity of the –OH and –COOH groups

facilitates a strong intramolecular hydrogen bond. This bond stabilizes the conjugate base formed after the first deprotonation, contributing to its pKa_1 of 2.98. In contrast, the *m*– and *p*–hydroxybenzoic acids cannot form such intramolecular hydrogen bonds, as their functional groups are separated by one or more carbon atoms. The pKa_1 values for *m*– and *p*–hydroxybenzoic acid are 4.08 and 4.57, respectively, which are higher than the pKa_1 value of the *o*–hydroxybenzoic acid due to the absence of intramolecular hydrogen bonding stabilization of the carboxylate anion. The internal hydrogen bond of *o*–hydroxybenzoic acid also makes the phenolic –OH group in *o*–hydroxybenzoic acid less acidic (pKa_2 *o*–hydroxybenzoic acid = 13.6) and stabilizes its conjugate base after the first deprotonation [24,25,26]. The pKa_2 of *o*–hydroxybenzoic acid is higher than the pKa_2 value of its isomers, which are 9.92 for *m*-hydroxybenzoic acid and 9.46 for *p*-hydroxybenzoic acid. The higher pKa_2 value indicates that deprotonation of the phenolic –OH in *o*–hydroxybenzoic acid requires a more alkaline environment, consistent with the observed optimum pH of 11 during AuNPs synthesis. At this pH, the speciation profile derived from its pKa_2 shows that *o*–hydroxybenzoic acid is dominantly present as a mono-deprotonated species. In contrast, the *m*–hydroxybenzoic acid and *p*–hydroxybenzoic isomers, where the –OH and –COOH groups are separated by one or more carbon atoms, cannot form intramolecular hydrogen bonds. Optimum synthesis pH of *m*– and *p*–hydroxybenzoic around 10, –OH groups of these isomers remain largely in their fully protonated species. The absence of intramolecular stabilization makes deprotonation and subsequent reduction proceed effectively under slightly less alkaline conditions.

The effect of pH was found to play a central role not only in controlling the Au^{3+} reduction process but also in determining the degree of stabilization. The higher pKa_2 of *o*–hydroxybenzoic acid is not only a chemical constant but also a reflection of its intramolecular hydrogen bonding strength, which in turn governs its reduction behavior, coordination ability, and overall effectiveness as a dual reducing-capping agent for AuNPs synthesis.

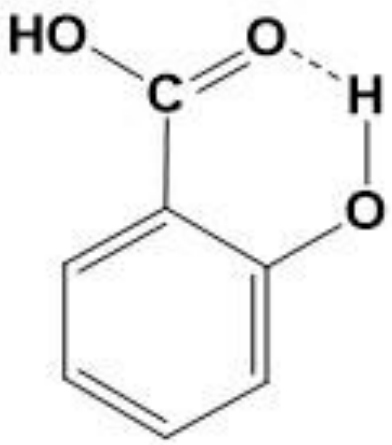


Figure 2 The intramolecular hydrogen bonds responsible for stabilizing *o*–hydroxybenzoic acid.

Fourier transmission infrared (FTIR) spectrophotometer

The FTIR spectra of the three hydroxybenzoic acid isomers (*o*–, *m*–, and *p*–hydroxybenzoic acid) illustrated in **Figure 3** and their corresponding hydroxybenzoic-capped AuNPs conjugates reveal clear spectral changes associated with the carbonyl ($C=O/COO^-$) and aromatic C=C vibrational regions. These changes provide important evidence of capping agent binding and surface interaction between hydroxybenzoic acid molecules and the AuNPs. For all isomers, the characteristic C=O stretching band of the free carboxylic acid is typically observed around 1,680 - 1,710 cm^{-1} either decreases markedly in intensity or shifts to lower wavenumber after nanoparticle formation. At the same time, two new bands emerge in the regions of 1,649 - 1,612 cm^{-1} and 1,400 - 1,360 cm^{-1}, which correspond to the asymmetric and symmetric stretching modes of the carboxylate

(COO^-) group. The appearance of these COO^- bands, accompanied by the attenuation of the original C=O vibration, suggests deprotonation of the carboxyl group during the reduction capping process and subsequent coordination of the carboxylate to the Au surface [28–30].

In the spectrum of free *o*–hydroxybenzoic acid (**Figure 3(a)**), the O–H stretching vibration appears as a broad and relatively weak band centered around 3,450 cm^{-1}, indicating an intramolecular hydrogen bond between the adjacent –OH and –COOH groups. Upon AuNPs capping, this band becomes even broader and less intense, suggesting that the intramolecular hydrogen bond is largely preserved. By contrast, free *m*– and *p*–hydroxybenzoic acids (**Figures 3(b) - 3(c)**) exhibit sharper and more intense O–H stretching bands, reflecting the absence of intramolecular hydrogen bonding and the presence of free or intermolecularly bonded –OH groups. After AuNP formation, the O–H band becomes even broader and less intense, indicating that the intramolecular hydrogen bond is largely preserved upon absorption, while partial deprotonation of the –OH group may occur under alkaline synthesis conditions (pH 11).

The FTIR spectrum of *o*–hydroxybenzoic acid exhibits characteristic bands at approximately 1,658 cm^{-1}, attributable to C=O stretching vibration of carboxylic acid group, along with bands at 1,612 and 1,573 cm^{-1} corresponding to aromatic C=C stretching modes. Additional vibrations in the region of 1,481 - 1,381 cm^{-1} are associated with phenyl ring vibrations and C–O stretching. Upon formation of *o*–hydroxybenzoic acid-capped AuNPs, several notable spectral changes are observed. The intense C=O stretching band of *o*–hydroxybenzoic acid shifts to 1,627 cm^{-1}, accompanied by a reduction in intensity and partial broadening. This shift is indicative of the coordination of the carboxylate group to the AuNPs surface. Simultaneously, the emergence and intensification of bands at 1,589 and 1,489 cm^{-1} suggest perturbations of the aromatic ring vibrations, consistent with electronic redistribution upon adsorption to the metallic surface. The band at 1,381 cm^{-1}, commonly assigned to symmetric stretching of the carboxylate ($–COO^-$), becomes more pronounced, supporting deprotonation and surface anchoring via the carboxylate group. In the case of *m*–hydroxybenzoic acid, the FTIR spectrum shows the C=O stretching band at 1,693 cm^{-1}, along with the aromatic C=C stretching band at 1,601 and 1,465 cm^{-1}. Following AuNPs formation, the C=O band shifted to 1,649 cm^{-1}, accompanied by intensified bands at 1,553 and 1,391 cm^{-1}. These changes support coordination of *m*–hydroxybenzoic acid to the AuNPs surface, primarily through the carboxylate group. However, compared to the *o*–hydroxybenzoic acid system, the magnitude of the C=O shift and perturbation of aromatic C=C bands are less pronounced.

The FTIR spectrum of *p*-hydroxybenzoic acid shows a strong C=O stretching band at 1,674 cm^{-1}, along with aromatic C=C vibrations at 1,581 and 1,512 cm^{-1}. Bands in the region of 1,450 - 1,419 cm^{-1} correspond to ring vibrations and C–O stretching modes. Upon *p*–hydroxybenzoic acid capped AuNPs, the C=O stretching band shifted to 1,612 cm^{-1}, indicating coordination of the carboxylate group to the AuNPs surface. The appearance of bands at 1,550 and 1,381 cm^{-1} is consistent with asymmetric and symmetric stretching of COO^- groups, indicating deprotonation and surface adsorption. However, compared to *o*–hydroxybenzoic acid, *m*– and *p*–hydroxybenzoic acids capped AuNPs have broader bands and smaller shifts, which implies weaker binding strength and greater conformational freedom.

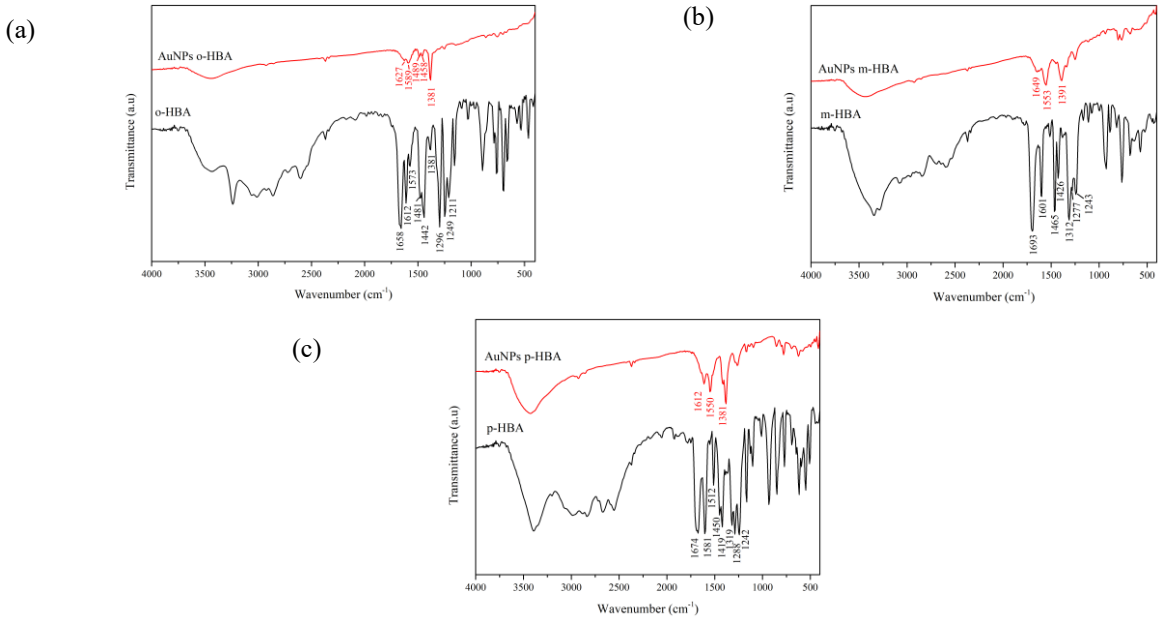


Figure 3 FTIR spectra of (a) *o*–hydroxybenzoic acid-capped AuNPs and *o*–hydroxybenzoic acid, (b) *m*–hydroxybenzoic acid-capped AuNPs and *m*–hydroxybenzoic acid, (c) *p*–hydroxybenzoic acid-capped AuNPs and *p*–hydroxybenzoic acid.

X- ray diffraction (XRD)

The crystalline nature of the synthesized AuNPs was confirmed through XRD analysis. The XRD pattern of *o*–, *m*–, and *p*–hydroxybenzoic acids-capped AuNPs (**Figure 4)** exhibit a series of characteristic diffraction peaks at 2θ: 38.2°, 44.4°, 64.6°, and 77.5°, which can be indexed to the (111), (200), (220), and (311) planes of face centered cubic (fcc) metallic gold (JCPDS No. 04-0784). Among these reflections, the intense diffraction peak corresponding to the (111) plane indicates the preferential orientation and high crystallinity of the synthesized AuNPs. No additional diffraction peaks associated with Au oxides or other crystalline impurity phases were observed in the *m*– and *p*–hydroxybenzoic acids-capped AuNPs, indicating the formation of phase-pure metallic AuNPs.

The XRD pattern of *o*–hydroxybenzoic acid-capped AuNPs exhibits several additional low-angle diffraction peaks in the 2θ region of approximately 12° and 25°. These peaks are absent in the *m*– and *p*–hydroxybenzoic acids capped AuNPs system and may originate from residual crystalline domains or ordered molecular packing of *o*–hydroxybenzoic acid on the nanoparticle surface. Previous studies have reported that crystalline *o*–hydroxybenzoic acid exhibits characteristic diffraction peaks in the low-angle region, particularly around 2θ = 12° and 25°, associated with its ordered crystal structure and intermolecular hydrogen-bonding arrangement [31–33]. The appearance of these additional reflections in the *o*–hydroxybenzoic acid-capped AuNPs may therefore suggest stronger surface organization or residual crystalline ordering promoted by the intramolecular hydrogen-bonding characteristic of the *o*– isomer. The dominant diffraction peaks in all samples remain characteristic of fcc metallic Au, indicating that positional isomerism primarily influences surface interaction and capping organization rather than the crystal structure of the AuNPs core itself.

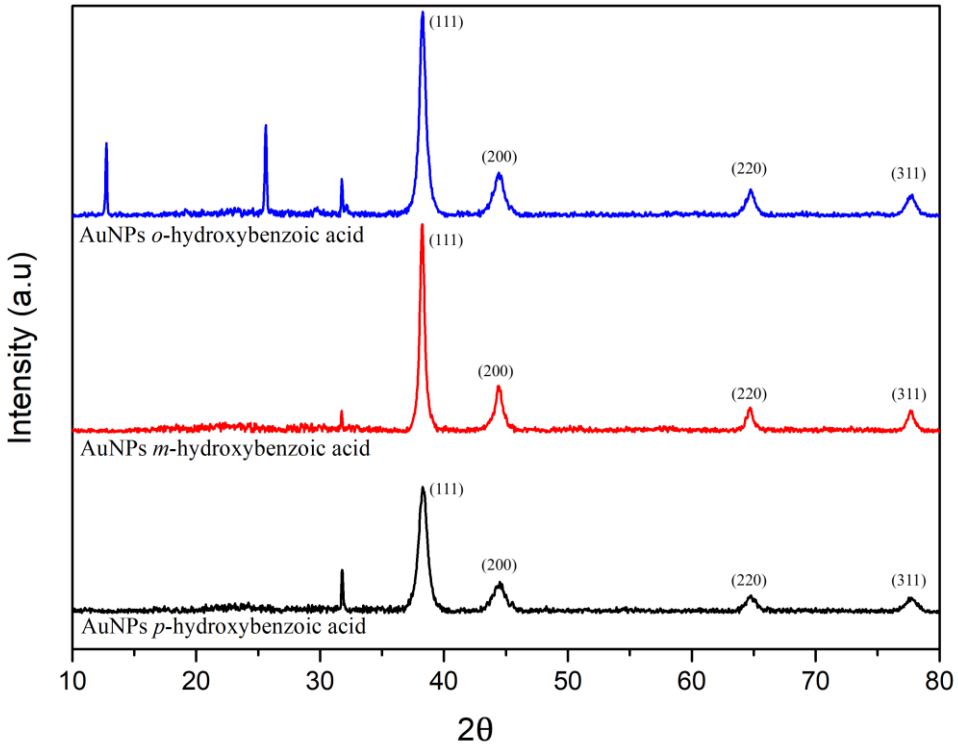


Figure 4 XRD pattern of *o*–, *m*–, and *p*–hydroxybenzoic acids-capped AuNPs.

Transmission electron microscope (TEM)

TEM analysis revealed clear differences in the morphology and size distribution of AuNPs synthesized using the three hydroxybenzoic acid isomers illustrated in **Figures 5(a)** - **(5c)** TEM images of AuNPs capped with *o*–hydroxybenzoic acid show predominantly spherical nanoparticles with relatively uniform size. The corresponding particle size histogram shows a narrow distribution centered at an average diameter of 22.28 nm, indicating a high degree of monodispersity. The relatively discrete particle boundaries observed in TEM further support the presence of a compact and rigid capping layer. AuNPs capped with *m*–hydroxybenzoic acid exhibit larger particle sizes and broader size distribution, with an average diameter of 33.50 nm. TEM images show partial aggregation and less uniform particle morphology, indicating reduced overgrowth of nanoparticles. AuNPs capped *p*–hydroxybenzoic acid show an average particle diameter of 33.49 nm, comparable to that of *m*–hydroxybenzoic acid-capped AuNPs. The particle size distribution is broader and skewed toward larger diameters, indicating a higher degree of polydispersity.

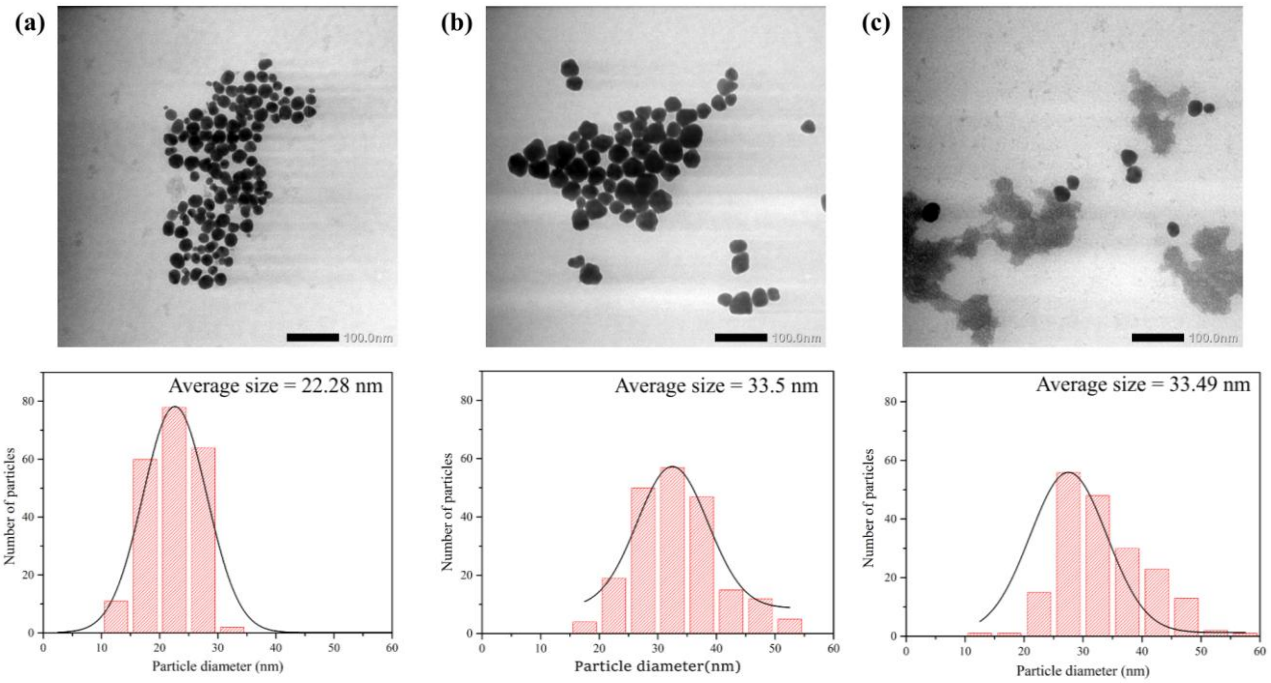


Figure 5 TEM images and distribution size of (a) *o*–hydroxybenzoic acid-capped AuNPs, (b) *m*–hydroxybenzoic acid-capped AuNPs, (c) *p*–hydroxybenzoic acid-capped AuNPs.

Dynamic light scattering (DLS) or particle size analysis (PSA)

DLS or PSA showed larger hydrodynamic diameters (**Figure 6**) compared to TEM measurements for all AuNPs. It should be noted that PSA/DLS measures the hydrodynamic diameter that is the particle core + organic capping layer + solvate/ionic layer that moves with the particles in solution, while TEM yields the size of the dry core scanned under vacuum. Therefore, PSA values are typically larger than TEM, and this difference is magnified when there is a thick organic layer or light aggregations that are not readily visible in TEM [25,26]. The *o*–hydroxybenzoic capped AuNPs shows an average hydrodynamic diameter of 46.76 ± 0.13 nm with a polydispersity index (PDI) of 0.24, whereas noticeably larger sizes are observed for *m*–hydroxybenzoic acid capped AuNPs (78.74 ± 0.28 nm, PDI = 0.14) and *p*–hydroxybenzoic acid capped AuNPs (58.09 ± 0.67 nm, PDI = 0.21). The PDI value for all three formulation are below 0.4, indicating that the nanoparticles are well dispersed and relatively monodisperse in aqueous media [34]. When compared with TEM-derived core sizes (around 22 nm for *o*–, and 33 for *m*–and *p*–hydroxybenzoic acid-capped AuNPs), all samples show the expected increase in size under solvated conditions, which is consistent with the presence of an organic capping layer and a hydration shell. However, the magnitude of this increase varies markedly among the isomers; the relatively modest hydrodynamic size of *o*–hydroxybenzoic capped AuNPs suggests the formation of a compact and tightly bound capping layer, which limits solvent penetration and suppresses interparticle association. In contrast, the substantially larger hydrodynamic diameter observed for *m*–hydroxybenzoic acid-capped AuNPs indicates a looser surface coverage and enhanced interparticle interaction. The *p*–hydroxybenzoic acid shows intermediate behavior, with a hydrodynamic size smaller than *m*–hydroxybenzoic but it is still larger than *o*–hydroxybenzoic systems. These findings demonstrate that hydrodynamic size is governed not only by the metallic core diameter but also by capping agent density and surface rigidity, which are strongly influenced by substituent positioning on the aromatic ring.

Zeta potential

The colloidal stability of AuNPs was further evaluated by measuring their zeta potential. In general, zeta potential reflects the surface charge of nanoparticles and is a crucial factor determining colloidal stability

[26,27]. All three samples of *o*–, *m*– and *p*–hydroxybenzoic acids capped AuNPs exhibited strongly negative surface charges, with average zeta potential value of −52.8 ± 1 mV, −51.5 ± 1.2 mV, and −52.1 ± 2.1 mV, respectively (**Figure 6**). These values fall well below the commonly accepted threshold of ± 30 mV for electrostatically stable colloids, indicating that systems possess excellent dispersion stability in aqueous media [31–33,35]. The high negative charge originates from the deprotonated carboxyl groups of the hydroxybenzoic, which create strong electrostatic repulsion between particles and effectively suppress aggregation. Although the three isomers show only slight differences in zeta potential, the *o*–hydroxybenzoic acid-capped AuNPs exhibited the most negative value (approximately -52.8 ± 1 mV), indicating strong interparticle electrostatic repulsion, effectively preventing aggregation. This result suggests that the neighboring –OH and –COOH groups in *o*–hydroxybenzoic acid provide strong anchoring and deprotonation, thereby increasing the negative charge density on the nanoparticle surface. In comparison, AuNPs capped with *m*–hydroxybenzoic acid indicating weaker electrostatic stabilization and explaining the relatively broad size distribution observed in the TEM and PSA result. *p*–hydroxybenzoic acid capped AuNPs exhibited an intermediate value (-52.1 ± 2.1 mV), consistent with moderate stability and particle size uniformity.

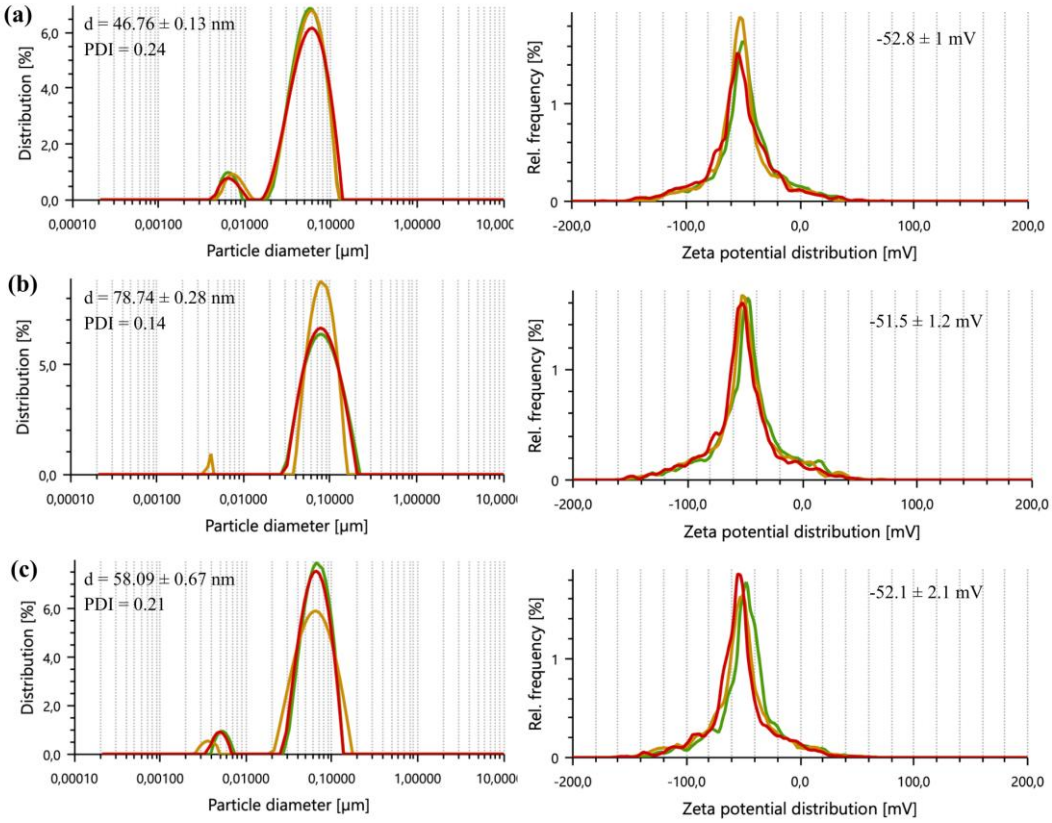


Figure 6 Dynamic light scattering and zeta potential of (a) *o*–hydroxybenzoic acid capped AuNPs, (b) *m*–hydroxybenzoic acid capped AuNPs, (c) *p*–hydroxybenzoic acid capped AuNPs.

The difference observed among the three isomers can be attributed to the relative position of the functional groups in the benzene ring. In the ortho isomer, the close proximity between the –OH and –COOH groups enables bidentate chelation and intramolecular hydrogen bonding, which strengthens the interaction with Au^{3+} ions and provides better control during nucleation. In contrast, the wider separation of these groups in *m*– and

p–hydroxybenzoic acids weakens their ability to coordinate with the metal ions, leading to the formation of larger and less uniformly distributed nanoparticles. This trend agrees with earlier reports showing that phenolic compounds with stronger chelating capability generally produce smaller and more monodisperse AuNPs [10,36,37].

Interactions of hydroxybenzoic acid isomer capped aunps with paraquat

UV-Vis spectrophotometer analysis

The interaction between paraquat and hydroxybenzoic acid isomers capped AuNPs was investigated using UV-Vis absorption spectroscopy. Measurement was performed 50 min after the addition of paraquat at various concentrations (1×10^{-4} - 1×10^{-3} M) to each colloidal suspension. Prior to paraquat addition, all three types of hydroxybenzoic acid capped AuNPs exhibit a single, well-defined SPR band in the wavelength range of 526 - 536 nm (**Figure 1**). Upon the addition of paraquat, the *o*–hydroxybenzoic acid-capped AuNPs exhibited concentration-dependent changes in the spectrum. As the paraquat concentration increased from 1×10^{-4} M to 1×10^{-3} M, the intensity of the original SPR band at approximately 526 - 536 nm progressively decreased. Simultaneously, a new broad absorption band appeared in the longer wavelength region between 650 and 800 nm (**Figure 7(a)**). This spectral change is characteristic of nanoparticle aggregation, where the proximity of adjacent particles induces plasmon coupling, resulting in the appearance of a red-shifted SPR band. The observed aggregation can be explained by the displacement or disruption of the *o*–hydroxybenzoic acid capping layer upon interaction with paraquat. *o*–hydroxybenzoic acid is known to form a stable intramolecular hydrogen bond, resulting in a rigid, cyclic structure that provides effective surface stabilization [12]. It is possible that the positively charged bipyridinium ions of paraquat may interact electrostatically with the negatively charged carboxylate groups on the AuNPs surface, potentially crosslinking adjacent nanoparticles and inducing aggregation [38]. The gradual increase in absorbance at 650 - 800 nm with increasing paraquat concentration is consistent with a progressive aggregation mechanism.

The *m*–hydroxybenzoic acid-capped AuNPs displayed a distinctly different spectral response to paraquat addition compared to their *ortho* position (**Figure 7(b)**). While a decrease in the intensity of the primary SPR band was observed with increasing paraquat concentration, the emergence of a secondary band in the 650 - 800 nm region was considerably less pronounced. This observation suggests that *m*–hydroxybenzoic acid-capped AuNPs less susceptible to paraquat-induced aggregation or undergo a different mode of interaction. *m*–hydroxybenzoic acid lacks the intramolecular hydrogen bond present in the *o*–isomer and exists as a mixture of conformers [12]. The capping layer formed by *m*–hydroxybenzoic acid may be less organized or provide different surface coverage, potentially resulting in a weaker interaction with paraquat molecules.

The *p*–hydroxybenzoic acid-capped AuNPs exhibited yet another distinctive response to paraquat (**Figure 7(c)**). Similar to the other isomers, a decrease in the primary SPR band intensity was observed with increasing paraquat concentration. However, the spectral changes, including the development of the red-shifted band, showed intermediate characteristics between the *o*– and *m*–isomers. *p*–hydroxybenzoic acid possesses a symmetric structure that allows for resonance delocalization across the entire molecule, enhancing its stability [10]. The capping layer formed by *p*–hydroxybenzoic acid may provide a different surface functionality compared to the other isomers. The observed spectral changes suggest that *p*–hydroxybenzoic acid-capped AuNPs do interact with paraquat and undergo aggregation, but the extent or nature of this aggregation differs from that observed with *o*–hydroxybenzoic acid.

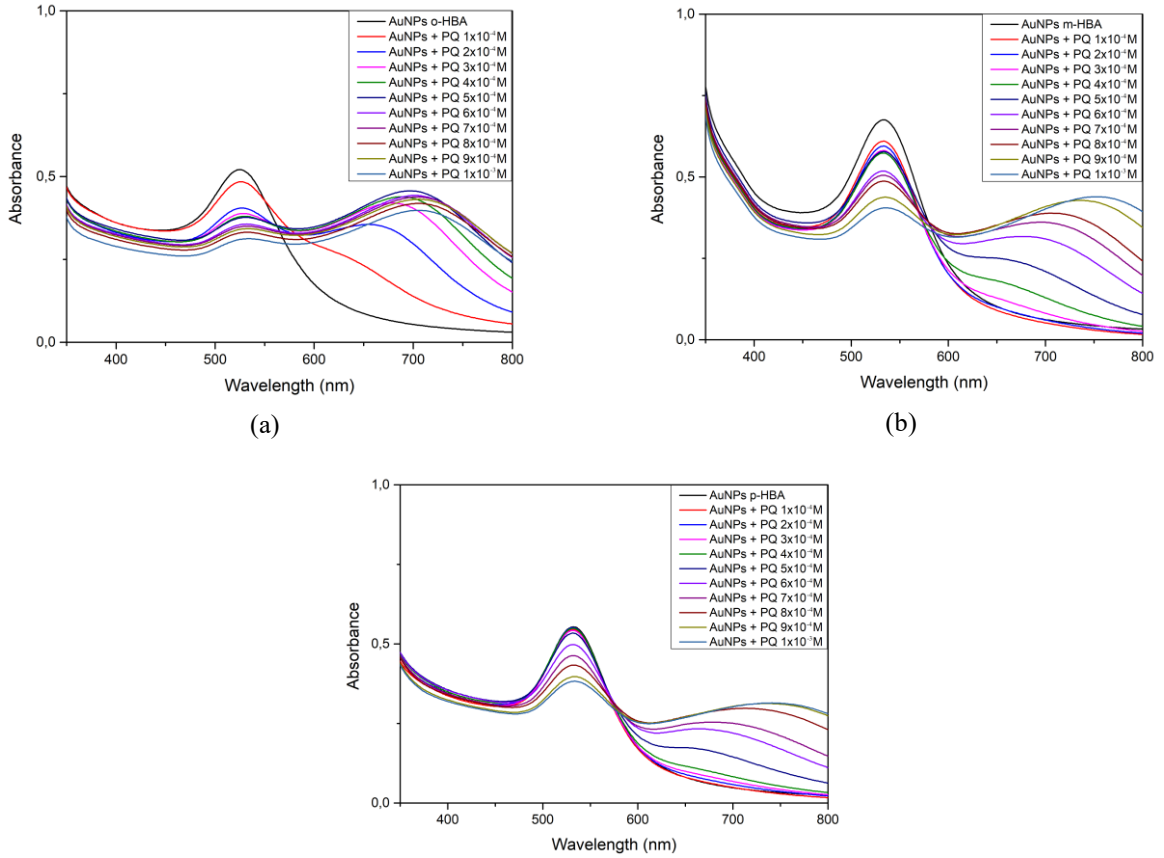


Figure 7 UV-Vis spectra of hydroxybenzoic acids-capped AuNPs after 50 min addition of paraquat at various concentrations (1×10^{-4} M - 1×10^{3} M): (a) *o*–hydroxybenzoic acid -capped AuNPs (b) *m*–hydroxybenzoic acid-capped AuNPs (c) *p*–hydroxybenzoic acid capped AuNPs.

TEM Analysis

Before the addition of paraquat, all three hydroxybenzoic acid isomers capped AuNPs exhibited predominantly spherical morphology with relatively narrow size distributions (**Figures 5(a) - 5(c)**). Upon addition of paraquat (**Figure 8**) all three types of hydroxybenzoic acid isomers capped AuNPs exhibited changes in their size distributions, although the extent and nature of these changes varied among the isomers. For *o*–hydroxybenzoic acid-capped AuNPs, the average particle size increased from 22.28 o 28.08 nm after paraquat exposure (**Figures 5(a)** and **8(a)**). This increase of approximately 5.8 nm represents the largest size change among the three isomers, indicating the highest degree of nanoparticle aggregation upon paraquat addition. The positively charged bipyridinium ions of paraquat likely interact electrostatically with the negatively charged groups on the AuNPs surface, potentially crosslinking adjacent nanoparticles and inducing aggregation [39]. The pronounced size increase observed for *o*–hydroxybenzoic acid-capped AuNPs can be attributed to the highly organized and exposed capping layer conformation resulting from intramolecular hydrogen bonding, which facilitates rapid and extensive interaction with paraquat, leading to massive and uncontrolled aggregation.

The *m*–hydroxybenzoic acid capped AuNPs showed a noticeable increase in particle size, increasing from 33.50 to 35.73 nm (**Figures 5(b)** and **8(b)**), an increase of approximately 2.22 nm. This moderate size increase is less pronounced than that of *o*–hydroxybenzoic acid-capped AuNPs. The flexible and less organized capping layer of *m*–hydroxybenzoic acid-capped AuNPs, resulting from the absence of intramolecular hydrogen bonding and the presence of multiple conformers, may provide weaker surface protection compared to *o*–hydroxybenzoic acid-capped AuNPs.

Interestingly, *p*–hydroxybenzoic acid-capped AuNPs exhibited a slight decrease in average size, from 33.49 to 31.94 nm (**Figures 5(c)** and **8(c)**), a reduction of approximately 1.55 nm. This unexpected observation may indicate that smaller nanoparticles within the population are preferentially involved in aggregation, leaving a population enriched in slightly larger particles. Alternatively, the dense capping layer of *p*–hydroxybenzoic acid resulting from strong intermolecular lateral interactions between adjacent ligand molecules may limit access of paraquat to the nanoparticle surface. Consequently, only the smallest particles within the polydisperse population undergo aggregation and subsequent sedimentation, while larger particles remain unaffected, which could explain an apparent decrease in the measured average particle size.

The differential responses observed by TEM are generally consistent with the UV-Vis spectroscopic data discussed previously. *o*–hydroxybenzoic acid capped AuNPs, despite having the smallest initial size (22.08 nm), exhibited the most noticeable size increase (5.8 nm) upon paraquat exposure, suggesting the greatest extent of aggregation. This finding is consistent with the UV-Vis analysis, where *o*–hydroxybenzoic acid-capped AuNPs showed rapid and pronounced spectral changes, characterized by a sharp decrease in the main SPR peak and the emergence of a broad peak in the 650 - 800 nm region. The substantial aggregation observed for *o*–hydroxybenzoic acid-capped AuNPs can be attributed to its highly organized capping layer with exposed carboxylate groups, which facilitates rapid and extensive electrostatic interaction with paraquat, leading to massive and uncontrolled aggregation.

From the TEM analysis results, it can be observed that the average distance between adjacent AuNPs decreased noticeably after the addition of paraquat. This reduction in interparticle distance was observed in all three isomers of hydroxybenzoic acid, although the degree of distance reduction varied depending on the structure of the capping agent. Before paraquat addition, AuNPs coated with *o*–, *m*–, and *p*–hydroxybenzoic acid appeared as well-dispersed individual particles with relatively uniform separation distances. The nanoparticles maintained sufficient spacing, indicating effective stabilization by the capping layers through electrostatic and steric repulsion mechanisms [40]. However, upon the addition of paraquat (**Figures 8(a)** - **8(c)**), a clear trend toward closer particle proximity is evident. The nanoparticles are observed in closer association, with some regions showing near contact or partial aggregation.

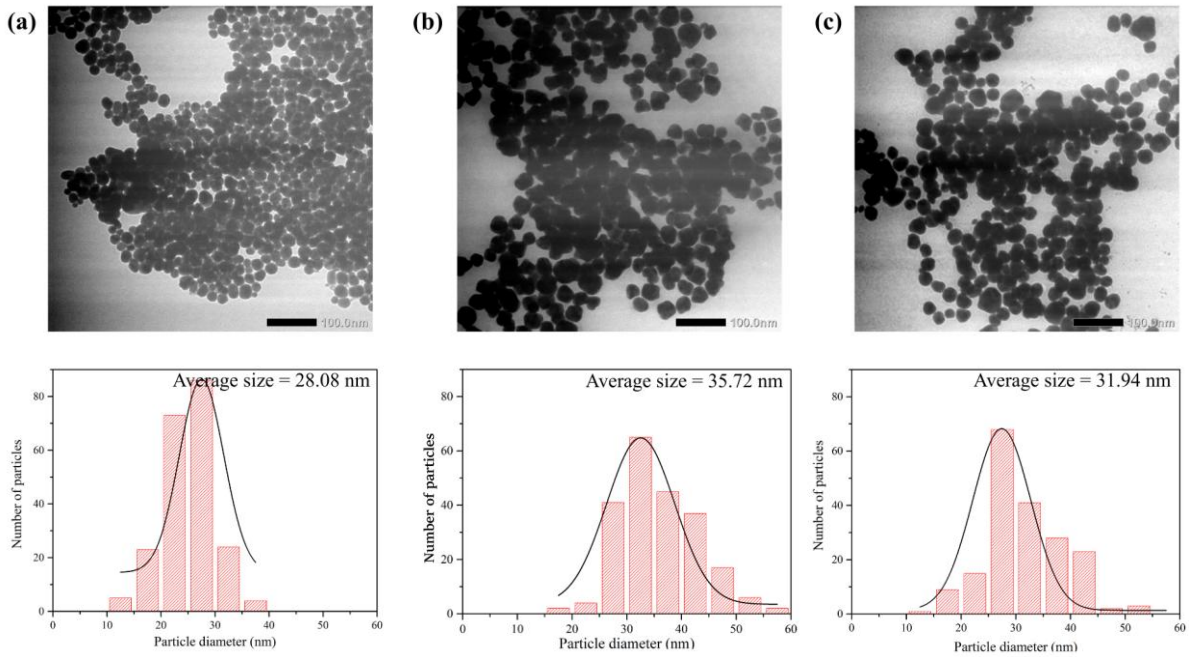


Figure 8 TEM images and distribution size of AuNPs capped with hydroxybenzoic isomers after interaction with paraquat: (a) *o*–hydroxybenzoic acid-capped AuNPs, (b) *m*–hydroxybenzoic acid-capped AuNPs, and (c) *p*–hydroxybenzoic acid-capped AuNPs.

Dynamic light scattering (DLS) or particle size analysis (PSA)

Figure 9 presents the particle size distribution profiles for hydroxybenzoic acid isomers capped AuNPs after exposure to paraquat. Before the addition of paraquat, all three hydroxybenzoic acid isomers capped AuNPs exhibited nanoparticle size distribution with average hydrodynamic diameters in the nanoparticle range (**Figure 6**). Upon addition of paraquat, all three hydroxybenzoic acids-capped AuNPs exhibited substantial increases in their average hydrodynamic diameters, indicating paraquat-induced aggregation. The *o*–hydroxybenzoic acid capped AuNPs showed a dramatic increase in hydrodynamic diameter from 46.76 ± 0.13 nm (PDI = 0.24) to 92.55 ± 0.64 nm (PDI = 0.25) upon paraquat addition, nearly doubling in size. This increase provides evidence of nanoparticles aggregation induced by paraquat. The aggregation mechanism involves electrostatic crosslinking, where the dicationic paraquat molecules bridge adjacent nanoparticle by interacting with the negatively charged carboxylate groups on the AuNPs surface [39,41,42].

The *m*–hydroxybenzoic acid capped AuNPs exhibited the largest absolute hydrodynamic diameter after paraquat addition (123.85 ± 3.08 nm, PDI = 0.27), representing an increase of approximately 45 nm from the initial size (**Figure 6(b)**). This marked increase suggests that *m*–hydroxybenzoic acid-capped AuNPs undergo paraquat-induced aggregation. However, the larger final hydrodynamic diameter of *m*–hydroxybenzoic acid-capped AuNPs compared to *o*–hydroxybenzoic acid-capped AuNPs does not necessarily indicate more extensive aggregation of the gold core. Instead, this difference is primarily attributed to the thicker and more hydrated capping layer of *m*–hydroxybenzoic acid-capped AuNPs, which likely contributes substantially to the hydrodynamic diameter measured by DLS, combined with its larger initial core size (33.5 nm from TEM) relative to *o*–hydroxybenzoic acid-capped AuNPs (22.28 nm from TEM). The flexible capping layer of *m*–hydroxybenzoic acid-capped AuNPs, resulting from the absence of intramolecular hydrogen bonding, facilitates controlled and progressive aggregation upon paraquat addition. Consequently, while *m*–hydroxybenzoic acid-capped AuNPs shows the largest hydrodynamic diameter after aggregation, this reflects its unique capping layer properties specifically greater thickness and hydration. The flexible capping layer of *m*–hydroxybenzoic acid capped AuNPs provides optimal steric stabilization and permitting paraquat induced crosslinking to occur in a concentration dependent manner.

The *p*–hydroxybenzoic acid-capped AuNPs showed the smallest increase in hydrodynamic diameter, from 58.09 ± 0.67 nm to 78.05 ± 0.65 nm (PDI = 0.20) (**Figures 6(c)** and **9(c)**), representing an increase of approximately 19.96 nm. This relatively modest increase suggests that *p*–hydroxybenzoic acid-capped AuNPs are the least susceptible to paraquat-induced aggregation compared to the other isomers. The symmetric structure and resonance delocalization in *p*–hydroxybenzoic acid capped AuNPs may contribute to a more stable capping layer that partially resists paraquat bridging. However, the increase in size is consistent with the occurrence of interaction with paraquat, albeit on a smaller scale. This finding shows general agreement with UV-Vis and TEM data, both of which suggest that *p*–hydroxybenzoic acid capped AuNPs exhibit the weakest interaction with paraquat among the three isomers. The PDI values for the three hydroxybenzoic acid-capped AuNPs systems after paraquat addition were bellow 0.4, indicating good colloidal monodispersity and size uniformity even though the particle size increased [34].

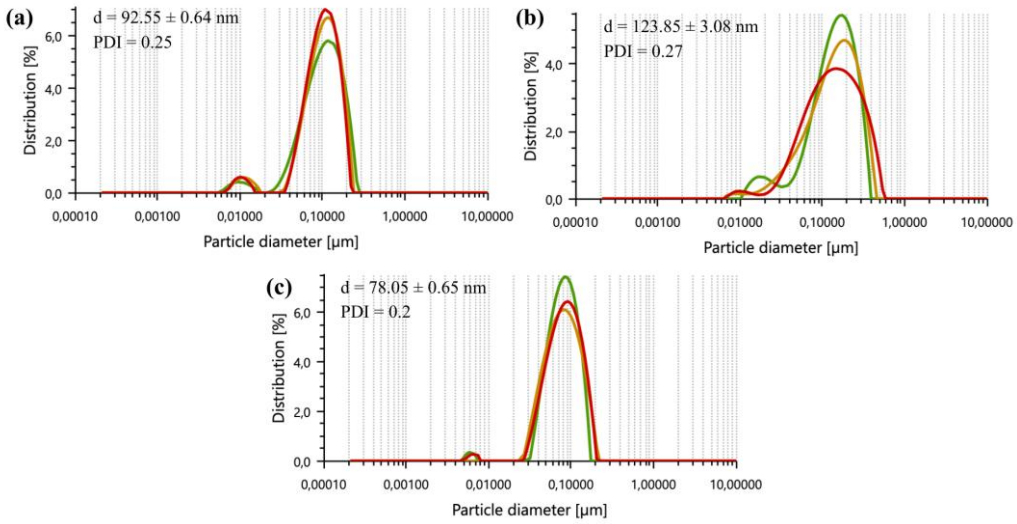


Figure 9 Dynamic light scattering of AuNPs capped hydroxybenzoic isomers after interaction with paraquat: (a) *o*–hydroxybenzoic acid-capped AuNPs, (b) *m*–hydroxybenzoic acid-capped AuNPs, (c) *p*–hydroxybenzoic acid-capped AuNPs.

Mechanistic insights into Paraquat-Hydroxybenzoic acid interaction: The role of π–π stacking and Host-Guest chemistry

To explore the possible molecular basis of the interaction between hydroxybenzoic acid isomers capped AuNPs with paraquat, it is useful to consider the potential noncovalent interactions that may be involved. When *o*–, *m*–, or *p*–hydroxybenzoic acid binds to the AuNPs surface via $–COO^-$ or –OH group, its aromatic ring remains exposed to the surrounding medium, potentially allowing it to interact with other aromatic moieties near the nanoparticle. Phenolic compounds adsorbed on AuNPs may retain a degree of π–donor character and could participate in interactions with charged aromatic species. Paraquat (1,1′-dimethyl-4,4′-bipyridinium dichloride) is a dicationic bipyridinium molecule ($^{2+}$), which makes its aromatic framework electron deficient (π–deficient). As a result, paraquat has the potential to engage in donor–acceptor interactions with π–rich aromatic systems, such as benzene, phenolic rings, and substituted benzoic acid derivatives. According to the reference [42], π–π stacking interactions are generally described as occurring when aromatic π systems bind in a face-to-face manner, involving a combination of dispersion and dipole-induced dipole interactions. Such π–donor–acceptor interaction, if present, could contribute to the binding between paraquat and the hydroxybenzoate capping layer.

In the present AuNPs-paraquat system, the hydroxybenzoic acid-capped AuNPs surface may be conceptually viewed as a host, potentially providing a binding pocket for paraquat as the guest. In host-guest chemistry, a large molecule or network host can noncovalently bind a smaller guest molecule within a binding pocket. In principle, various types of intermolecular interaction may contribute to holding a host-guest complex together. When a conformationally flexible host binds a guest, a considerable amount of conformational entropy can be lost, which may disfavor binding. To mitigate this, an effective host is typically designed to minimize the loss of conformational entropy by restricting its own conformational flexibility from the outset. Xiong, *et al.*[38] demonstrated that AuNPs functionalized with carboxylate-containing compounds exhibit high selectivity toward paraquat, which they attributed to host-guest recognition mechanisms.

In the *o*–hydroxybenzoic acid-paraquat illustration (**Figure 10(a)**), the aromatic ring of *o*–hydroxybenzoic acid is shown in close proximity to one of the pyridinium rings of paraquat. The curved lines between the rings are intended to represent a possible π–π stacking interaction. The *o*–hydroxybenzoic acid molecule is depicted with its characteristic intramolecular hydrogen bond between the neighboring

–OH and –COOH groups, forming a rigid, cyclic structure. This conformation may present the aromatic ring in an orientation that could favor π–type interactions. The *m*–hydroxybenzoic acid–paraquat illustration (**Figure 10(b)**) similarly show the aromatic ring of *m*–hydroxybenzoic acid positioned near a pyridinium ring of paraquat, with curved lines indicating potential π–π interactions. However, *m*–hydroxybenzoic acid lacks the intramolecular hydrogen bond present in the *ortho* isomer; it exhibits greater conformational flexibility. This flexibility may affect the orientation and stability of the π–π interaction with paraquat. The *p*–hydroxybenzoic acid-paraquat illustration (**Figure 10(c)**) depicts that the symmetric *p*–hydroxybenzoic acid allows resonance delocalization across the molecule, which may influence its electron density distribution, and consequently, its potential to engage in π–π interactions with paraquat.

While the proposed π–π interaction mechanism is strongly supported by the observed concentration-dependent SPR shifts, hydrodynamic size enlargement, and interparticle distance reduction. We acknowledge that direct spectroscopic evidence (e.g., from Raman or surface-enhanced Raman scattering (SERS) spectroscopy) would further strengthen this interpretation, and this will be an important direction for future work.

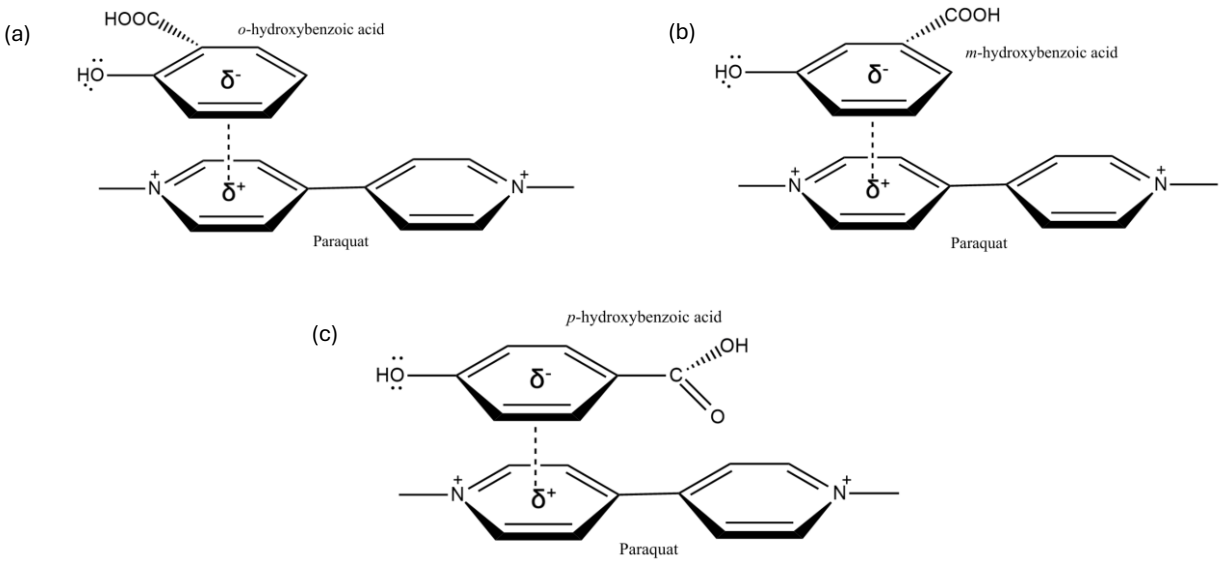


Figure 10 Illustration for π–π interaction of paraquat with (a) *o*–hydroxybenzoic acid; (b) *m*–hydroxybenzoic acid; or (c) *p*–hydroxybenzoic acid.

Each paraquat molecule, with its two aromatic pyridinium rings, could potentially simultaneously engage in π–π stacking with the aromatic ring of a hydroxybenzoic acid molecule located on two different AuNPs. If such dual interaction occurs, it could bridge adjacent nanoparticles and may contribute to the reduction of the interparticle distance. This possibility is illustrated schematically in **Figure 11**, where paraquat molecules are shown positioned between multiple AuNPs cores, with curved lines representing a potential π–interaction connecting to multiple particles.

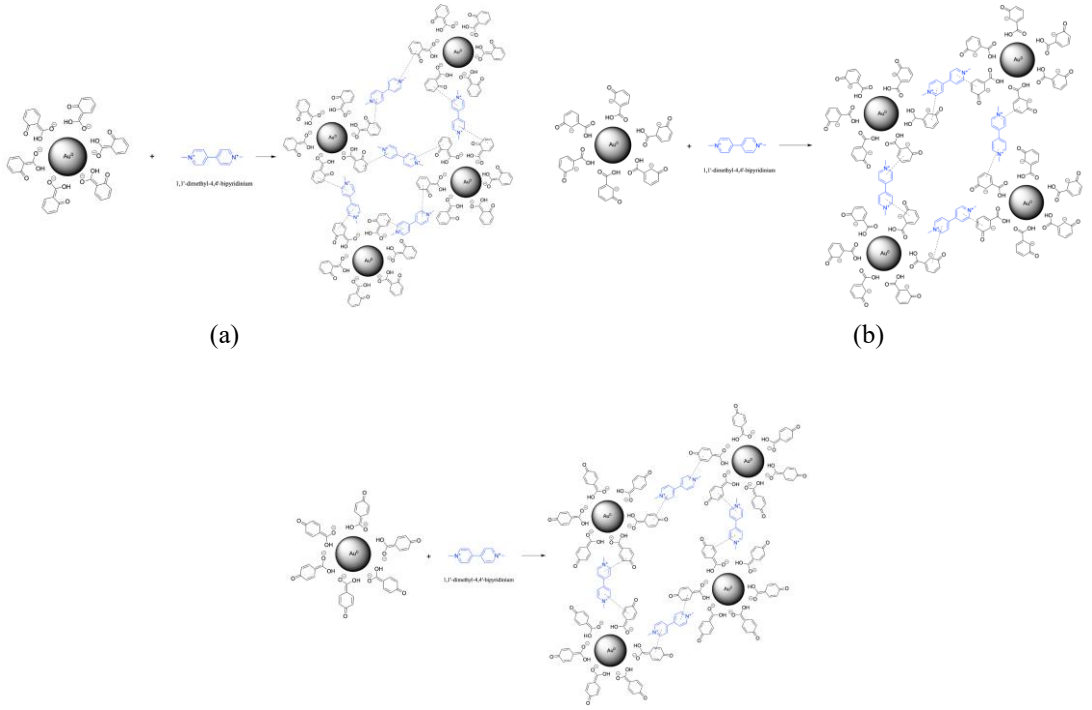


Figure 11 Schematic illustration of the interaction of paraquat with AuNPs capped by (a) *o*–hydroxybenzoic acid, (b) *m*–hydroxybenzoic acid, and (c) *p*–hydroxybenzoic acid.

Figure 11 provides a schematic representation of the proposed interaction mechanism between paraquat (1,1'-dimethyl-4,4'-bipiridinuim) and hydroxybenzoic acid isomers capped gold nanoparticle, suggesting a crucial role of positional isomerism in governing surface accessibility, interparticle bridging, and aggregation behavior. Based on the combined characterization result obtained from UV–Vis spectroscopy, TEM, and DLS/PSA measurements (shown in **Figures 1**, **5** and **6**), *o*–hydroxybenzoic acid-capped AuNPs exhibit smaller and more uniform particle sizes compared to those capped with *m*– dan *p*–hydroxybenzoic. This behavior is consistent with the presence of intramolecular hydrogen bonding in *o*–hydroxybenzoic acid, which appears to promote a more compact and rigid capping arrangement on the AuNPs surface, thereby contributing to enhanced colloidal stability relative to the other isomers. However, upon the introduction of paraquat, the stability of the *o*–hydroxybenzoic acid-capped AuNPs appears to become noticeably perturbed. Interestingly, UV–Vis spectra (**Figure 7**) reveal that the red shift of the SPR band is more pronounced for *o*–hydroxybenzoic acid-capped AuNPs than for the *meta* and *para* system, which may indicate a stronger optical response toward paraquat. This observation is consistent with the possibility that, despite their higher intrinsic stability, *o*–hydroxybenzoic acid-capped AuNPs may be particularly sensitive to paraquat-induced surface interaction.

In contrast, TEM and DLS/PSA analyses show that *m*–hydroxybenzoic acid-capped AuNPs possess larger particle sizes than the other systems, both before and after paraquat additions (**Figures 5** and **6**, **8** and **9**). This behavior is consistent with the synthesis results, which indicate that *m*–hydroxybenzoic acid-capped AuNPs are inherently larger and less monodisperse, likely due to weaker surface confinement during nanoparticle growth. Consequently, the larger size increase observed for *m*–hydroxybenzoic acid-capped AuNPs after paraquat exposure may reflect not only analyte-induced aggregation but also their initial size and polydispersity.

Quantitatively, TEM analysis indicates that both *o*– and *m*–hydroxybenzoic acids-capped AuNPs experience an increase in core particle size of approximately 2 nm after paraquat interaction (**Figure 8**), while DLS measurements reveal a much larger increase in hydrodynamic diameter of approximately 45 nm (**Figure 9**). This discrepancy is consistent with the

interpretation that paraquat may interact more strongly with *o*– and *m*– hydroxybenzoic acids-capped AuNPs, potentially through aromatic π–π stacking interactions, which could lead to the formation of crosslinked nanoparticle networks that contribute to the increased hydrodynamic radius. However, direct evidence (e.g., from Raman, SERS, or NMR) would be required to unambiguously confirm the π–π stacking mechanism. Notably, although *o*–hydroxybenzoic acid-capped AuNPs are expected to be more rigid and tightly packed due to intramolecular hydrogen bonding, they appear more susceptible to paraquat-induced perturbation. This behavior could be rationalized by the strong resonance effect in *o*–hydroxybenzoic acid, which may promote electron delocalization extending from the aromatic ring, potentially creating a more electron rich π environment [1,12]. Such an environment could, in principle, enhance the likelihood of π–π stacking interactions with the π deficient bipyridinium rings of paraquat, potentially facilitating effective surface-mediated interaction. Meanwhile, *p*–hydroxybenzoic acid-capped AuNPs, despite possessing resonance capability comparable to *o*–hydroxybenzoic acid [10], appear to exhibit a different interaction profile. When capped to the AuNPs surface, *p*–hydroxybenzoic acid molecule is likely to retain greater rotational freedom, and this conformational flexibility could potentially reduce the efficiency of face-to-face π–π stacking with paraquat. As a result, the *p*–hydroxybenzoic acid system shows a weaker plasmonic response and a smaller degree of aggregation compared to the *o*– and *m*–hydroxybenzoic acid-capped AuNPs.

Conclusions

The position isomerism of the hydroxyl acids strongly influences the formation, colloidal stability, and paraquat behavior of the resulting AuNPs. Among the three isomers, *o*–hydroxybenzoic acid produces the smallest (22.28 nm), and uniform AuNPs under the studied experimental condition, as indicate by their smaller particle size and higher negative zeta potential. In the absence of paraquat, all hydroxybenzoic acid-capped AuNPs systems remained relatively stable and exhibited characteristic SPR bands in the range of 526 - 536 nm. Upon paraquat addition (1×10^{-4} M - 1×10^{-3} M), concentration-dependent spectral changes, hydrodynamic size enlargement, and nanoparticle aggregation were observed, indicating destabilization of the colloidal systems. *o*–Hydroxybenzoic acid-capped AuNPs showed the most pronounced optical response toward paraquat, whereas *p*–hydroxybenzoic acid-capped AuNPs exhibited weaker aggregation behavior. The observed interaction behavior is proposed to involve electrostatic attraction and possible π–π donor–acceptor interaction between paraquat and the hydroxybenzoic acid capping layer. Overall, these findings demonstrate that hydroxybenzoic acid positional isomerism plays an important role in controlling AuNPs stability and paraquat-induced aggregation behaviour, providing a fundamental basis for the future development of AuNPs-based paraquat sensing systems.

Acknowledgements

The authors gratefully acknowledge the Indonesian Education Scholarship (BPI), Center for Higher Education Funding and Assessment (PPAPT), and Indonesian Endowment Fund for Education (LPDP) for providing a doctoral scholarship to Wianthi Septia Witasari and research funding under Decree No. 010587/PPAPT.1.2/BPI.06/02/2025.

Declaration of Generative AI in Scientific Writing

The authors acknowledge the use of generative AI tools (e.g., Grammarly, ChatGPT by openAI, Deepseek) in the preparation of this manuscript, specifically for language editing and grammar correction. No content generation or data interpretation was performed by AI. The authors take full responsibility for the content and conclusions of this work.

CRediT Author Statement

Wianthi Septia Witasari: Data curation, Formal analysis, Investigation, Resource, Visualization, Writing – original draft. **Adhitasari Suratman**: Validation, Writing - Review & Editing, Supervision. **Sri Juari Santosa**: Conceptualization, Methodology, Supervision, Validation, Writing – review and editing.

Reference

[1] MR Kumalasari, R Alfanaar and AS Andreani. Gold Nanoparticles (AuNPs): A versatile material for biosensor application. *Talanta Open* 2024; **9**, 100327.

[2] SAF Kusuma, JA Harmonis, R Pratiwi and AN Hasanah. Gold nanoparticle-Based colorimetric sensors: Properties and application in detection of heavy metals and biological molecules. *Sensors* 2023; **23(19)**, 8172.

[3] S Palani, JP Kenison, S Sabuncu, T Huang, F Civitci, S Esener and X Nan. Multispectral localized surface plasmon resonance (msLSPR) reveals and overcomes spectral and sensing heterogeneities of single gold nanoparticles. *ACS Nano* 2023; **17(3)**, 2266.

[4] DPS Negi. Recent developments in the colorimetric sensing of biological molecules using gold nanoparticles-based probes. *Talanta Open* 2022; **6**, 100122.

[5] H Kim, M Park, J Hwang, JH Kim, DR Chung, KS Lee and M Kang. Development of Label-free colorimetric assay for MERS-CoV using gold nanoparticles. *ACS Sensor* 2019; **4(5)**, 1306-1312.

[6] H Yuan, W Ji, S Chu, Q Liu, J Guang, G Sun, Y Zang, X Han, J Masson and W Peng. Au nanoparticles as label-free competitive reporters for sensitivity enhanced fiber-optic spr heparin sensor. *Biosensor and Bioelectronic* 2020; **154**, 112039.

[7] R D'Agata and G Spoto. Surface plasmon resonance imaging for nucleic acid detection. *Analytical and Bioanalytical Chemistry* 2013; **405**, 573-584.

[8] H Chen, S Cai, J Luo, X Liu, L Ou, Q Zhang, B Liedberg and Y Wang. Colorimetric biosensing assays based on gold nanoparticles functionalized/combined with non-antibody recognition elements. *Trends in Analytical Chemistry* 2024; **173**, 117654.

[9] SM Amini and A Akbari. Metal nanoparticles synthesis through natural phenolic acids. *IET Nanobiotechnology* 2019; **13(8)**, 771-777.

[10] AS Andreani, ES Kunarti and SJ Santosa. Synthesis of gold nanoparticles capped-benzoic acid derivative compounds (o-, m-, and p-Hydroxybenzoic Acid). *Indonesian Journal of Chemistry* 2019; **19(2)**, 376.

[11] AM Figat, B Bartosewicz, M Liszewska, B Budner, M Norek and BJ Jankiewicz. α-Amino Acids as Reducing and Capping Agents in Gold Nanoparticles Synthesis Using the Turkevich Method. *Langmuir* 2023; **39(25)**, 8646-8657.

[12] A Hill, H Sa'Adeh, D Cameron, F Wang, AB Trofimov, EY Larionova, R Richter and K Prince. Positional and conformational isomerism in hydroxybenzoic acid: A Core-level study and comparison with phenol and benzoic acid. *Journal of Physical Chemistry A* 2021; **125(45)**, 9877-9891.

[13] K Aarset, EM Page and DA Rice. Molecular structures of benzoic acid and 2-Hydroxybenzoic acid, obtained by gas-phase electron diffraction and theoretical calculations. *Journal of Physical Chemistry A* 2006; **112(40)**, 10040-10045.

[14] K Aarset, EM Page and DA Rice. Molecular structures of 3-hydroxybenzoic acid and 4-hydroxybenzoic acid, obtained by gas-phase electron diffraction and theoretical calculations. *Journal of Physical Chemistry A* 2008; **112(40)**, 10040.

[15] P Kongpreecha and S Siri. Simple colorimetric screening of paraquat residue in vegetables evaluated by localized surface plasmon resonance of gold nanoparticles. *Biotechnology and Applied Biochemistry* 2022; **69(3)**, 1148-1158.

[16] H Liu, Q Wu, T Chu, Y Mo, S Cai, M Chen and G Zhu. High-dose acute exposure of paraquat induces injuries of swim bladder, gastrointestinal tract and liver via neutrophil-mediated ROS in zebrafish and their relevance for human health risk assessment. *Chemosphere* 2018; **205**, 662-673.

[17] M Abbaszadeh, MH Sayadi and J Kharkan. Impact of polyvinyl chloride microplastic and paraquat herbicide on the blood cells, biochemical parameters, liver enzymes and morphological changes of aqueduct fish. *Chemosphere* 2024; **362**, 142643.

[18] P Sharma and P Mittal. Parkinsonism and related disorders paraquat (herbicide) as a cause of Parkinson's Disease. *Parkinsonism and Related Disorders* 2024; **119**, 105932.

[19] J Wu, W Shao, X Liu, F Zheng, Y Wang, P Cai, Z Guo, H Hu, G Yu, J Guo, L Yao, S Wu and H Li. Microglial exosomes in Paraquat-Induced Parkinson's disease: Neuroprotection and biomarker clues. *Environmental Pollution* 2024; **352**, 124035.

[20] J Turkevich, PC Stevenson and J Hillier. A study of the nucleation and growth processes in the synthesis of colloidal gold. *Discussion of the Faraday Society* 1951; **11**, 55-75.

[21] W Haiss, NTK Thanh, J Aveyard and DG Fernig. Determination of size and concentration of gold nanoparticles from UV-Vis spectra. *Analytical Chemistry* 2007; **79(11)**, 4215-4221.

[22] G Gusrizal, SJ Santosa, ES Kunarti and B Rusdiarso. Dual function of p-Hydroxy benzoic acid as reducing and capping agent in rapid and simple formation of stable silver nanoparticles. *International Journal of Chemtech Research* 2016; **9(09)**, 472-482.

[23] G Gusrizal, SJ Santosa, ES Kunarti and B Rusdiarso. Synthesis of silver nanoparticles by reduction of silver ion with m-hydroxybenzoic acid. *Asian Journal of Chemistry* 2017; **29(7)**, 1417-1422.

[24] P Kongpreecha and S Siri. A new colorimetric aptasensor for paraquat detection based on the designed aptamer with multiple paraquat binding sites in combination with gold nanoparticles. *Analytical Methods* 2024; **16(15)**, 2340-2348.

[25] R Fujiki, T Matsui, Y Shigeta, H Nakano and N Yoshida. Recent developments of computational methods for pKa prediction based on electronic structure theory with solvation models. *J* 2021; **4(4)**, 849-864.

[26] J Stetefeld, SA McKenna and TR Patel. Dynamic light scattering: A practical guide and applications in biomedical sciences. *Biophysical Reviews* 2016; **8(4)**, 409-427.

[27] S Mourdikoudis, RM Pallares and NTK Thanh. Characterization techniques for nanoparticles: Comparison and complementarity upon studying nanoparticle properties. *Nanoscale* 2018; **10(27)**, 12871.

[28] X Jiang, W Zhang, S Zhao, S Zhou, Y Shi and Z Xin. Effect of benzoic acid surface modified alumina nanoparticles on the mechanical properties and crystallization behaviour of isotactic polypropylene nanocomposites. *RSC Advances* 2018; **8(37)**, 20790-20800.

[29] P Wulandari, T Nagahiro, K Michioka, K Tamada, KI Ishibashi, Y Kimura and M Niwano. Coordination of carboxylate on metal nanoparticles characterized by fourier transform infrared spectroscopy. *Chemistry Letter* 2008; **37(8)**, 888-889.

[30] P Wulandari, T Nagahiro, N Fukada, Y Kimura, M Niwano and K Tamada. Characterization of citrates on gold and silver nanoparticles. *Journal of Colloid and Interface Science* 2015; **438**, 244-248.

[31] I Sathisaran and SV Dalvi. Crystal engineering of curcumin with salicylic acid and hydroxyquinol as coformers. *Crystal Growth and Desain* 2017; **17(7)**, 3974-3988.

[32] M Stec and PM Synowiec. Precipitation of salicylic acid with and without US-assistance. study on supersaturation discharge, cconversion, and yield. *Chemical Engineering and Processing - Process Intensification* 2026; **226**, 110847.

[33] TN Caio, N Gonçalves, F Wypych and LMF Lona. Enhancement of mechanical and thermal properties of poly(L-lactide) nanocomposites filled with synthetic layered compounds. *International Journal of Polymer Science* 2017. https://doi.org/10.1155/2017/1985078.

[34] G Lanza, D Betancourth, A Avila, H Riascos and JA Perez-Taborda. Control of the size distribution of AuNPs for colorimetric sensing by pulsed laser ablation in liquids. *Kuwait Journal of Science* 2025; **52(1)**, 100294.

[35] S Bhattacharjee. DLS and zeta potential – What they are and what they are not? *Journal of Controlled Release* 2016; **235**, 337-351.

[36] HS Kim, YS Seo, K Kim, JW Han, Y Park and S Cho. Concentration effect of reducing agents on green synthesis of gold nanoparticles: Size, morphology, and growth mechanism. *Nanoscale Research Letter* 2016; **11**, 230.

[37] ECBA Alegria, APC Ribeiro, M Mendes, AM Ferraria, AMBD Rego and AJL Pombeiro. Effect of phenolic compounds on the synthesis of gold nanoparticles and its catalytic activity in the

reduction of nitro compounds. *Nanomaterials* 2018; **8(5)**, 320.

[38] Y Xiong, T Ma, H Zhang, L Qiu, S Chang, Y Yang and F Liang. Gold nanoparticle functionalized nanopipette sensors for electrochemical paraquat detection. *Microchimica Acta* 2022; **189**, 251.

[39] H Li, DX Chen, YL Sun, YB Zheng, LL Tan, PS Weiss and YW Yang. Viologen-mediated assembly of and sensing with carboxylatopillar[5]arene-modified gold nanoparticles. *Journal of the American Chemical Society* 2013; **135(4)**, 1570-1576.

[40] KJM Bishop, CE Wilmer, S Soh and BA Grzybowski. Nanoscale forces and their uses in self-assembly. *Small* 2009; **5(14)**, 1600-1630.

[41] C Kuitio, S Klangprapan, N Chingkitti, S Boonthavivudhi and K Choowongkomon. Aptasensor for paraquat detection by gold nanoparticle colorimetric method. *Journal of Environmental Science and Health B* 2021; **56(4)**, 370-377.

[42] K Haas. *CHEM 431: Inorganic chemistry (Haas)*. The LibreTexts libraries, Davis, California, 2020.